

NUMERICAL ANALYSIS OF REGULAR WAVES OVER AN ONSHORE OSCILLATING WATER COLUMN

D. P. Davyt, djavan_perez@hotmail.com

P.R.F. Teixeira, pauloteixeira@furg.br

Universidade Federal do Rio Grande - FURG, Av. Itália, km8, Campus Carreiros, 96201-900, Rio Grande, RS, Brazil

R. Ramalhais, ruben_ramalhais@hotmail.com

Universidade Nova de Lisboa, Faculdade de Ciências e Tecnologia, Monte de Caparica, 2829-516, Caparica, Portugal

E. Didier, edidier@lnec.pt

Laboratório Nacional de Engenharia Civil, Av. do Brasil, 101, 1700-066, Lisboa, Portugal

Abstract. *The potential of wave energy along coastal areas is a particularly attractive option in regions of high latitude, such as the coasts of northern Europe, North America, New Zealand, Chile and Argentina where high densities of annual average wave energy are found (typically between 40 and 100 kW/m of wave front). Power estimated in the south of Brazil is 30kW/m, creating a possible alternative of source energy in the region. There are many types and designs of equipment to capture energy from waves under analysis, such as the oscillating water column type (OWC) which has been one of the first to be developed and installed at sea. Despite being one of the most analyzed wave energy converter devices, there are few case studies using numerical simulation. In this context, the numerical analysis of regular waves over an onshore OWC is the main objective of this paper. The numerical models FLUINCO and FLUENT® are used for achieving this goal. The FLUINCO model is based on RANS equations which are discretized using the two-step semi-implicit Taylor-Galerkin method. An arbitrary lagrangean eulerian formulation is used to enable the solution of problems involving free surface movements. The FLUENT® code (version 6.3.26) is based on the finite volume method to solve RANS equations. Volume of Fluid method (VOF) is used for modeling free surface flows. Time integration is achieved by a second order implicit scheme, momentum equations are discretized using MUSCL scheme and HRIC (High Resolution Interface Capturing) scheme is used for convective term of VOF transport equation. The case study consists of a 10 m deep channel with a 10 m wide chamber at its end. One meter high waves with different periods are simulated. Comparisons between FLUINCO and FLUENT results are presented. Free surface elevation inside the chamber; velocity distribution and streamlines; amplification factor (relation between wave height inside the chamber and incident wave height); phase angle (angular difference between the wave inside and outside the chamber); and sloshing parameter to quantify it inside the chamber are analysed. Finally, a discussion of the potential and limitations of each numerical model as well as the behaviour of the onshore OWC device is presented.*

Keywords: *wave energy, oscillating water column, numerical simulation, finite element method, finite volume method*

1. INTRODUCTION

The wave energy along coastal areas in regions of high latitude, where annual average energy is between 40 and 100 kW/m of wave front, is a good alternative source. The potential of wave energy estimated in the south of Brazil is 30kW/m, creating a possible alternative of source energy in the region. Researchers at the *Universidade Federal do Rio Grande* (FURG), with the support of the Brazilian oil company Petrobras, investigated the energy potential and the feasibility of offshore and onshore installations near Rio Grande in Rio Grande do Sul state.

Based on various energy-extracting methods, a wide variety of systems has been proposed but only a few full-sized prototypes have been built and deployed in open coastal waters. Most of these are or were located on the shoreline or near shore, and they are sometimes named first generation devices. In general, these devices stand on the sea bottom or are fixed to a rocky cliff. Shoreline devices have the advantage of easier installation and maintenance, and do not require deep-water moorings and long underwater electrical cables. The typical first generation device is the oscillating water column (OWC) (Falcão, 2009).

The OWC device comprises a chamber partly submerged in a concrete or a steel structure in which there is an opening below the water surface. Air is trapped above the water free surface inside the chamber. Incident waves cause oscillation of the free surface inside this chamber, compressing and expanding the air above it, forcing it to flow through a turbine that drives an electrical generator. The axial-flow Wells turbine, which rotates continuously in one direction regardless of the direction of the air flow, is usually used for this purpose.

The first prototype of such system was developed at the end of the 80's, and full-sized prototypes were built in Tofteshallen (Norway), Sakata (Japan), Vizhinjam (India), Pico (Portugal) and Limpet (Scotland). The cross-sectional area of these OWCs (at mid water-free-surface level) lies in the range between 80–250 m². Their installed power capacity ranges from 60 to 500 kW (Falcão, 2009).

Theory regarding fixed OWC devices was first developed by Evans (1982) and Sarmento and Falcão (1985). Liu *et al.* (2009) analyzed the OWC device integrated with a breakwater using the FLUENT code. Horko (2007) also used the FLUENT code to optimize an OWC device according to the wave characteristics on the site. Barreiro *et al.* (2009) analysed the interaction among monochromatic waves and a point-absorption energy converter using the FLUENT code and obtained the water column response with wave frequency, identifying the resonance of the system. These studies tracked free surface elevation using the VOF (volume of fluid) model. Others, including Josset and Clément (2006), Brito-Melo (2000), Delauré and Lewis (2003) have used codes based on the Boundary Element Method.

Researches of this type of problem are closer to reality when a model that considers the complete Navier-Stokes equations is used. Therefore, two codes based on RANS equations are employed to simulate the action of regular waves on an OWC. The first, FLUINCO, is a code based on semi-implicit two-step Taylor-Galerkin method (Teixeira, 2001). The model adopts a tetrahedral linear element, which has the advantage to adapt to areas of complex geometry and to be an element of good computational efficiency. An arbitrary lagrangean eulerian (ALE) formulation is used to enable the solution of problems involving both large relative movement among bodies and surfaces, and movements of free surface. The spatial velocity mesh distribution is such that distortion of elements is minimized by smoothing through the use of functions that consider the influence of the velocity of each node belonging to boundary surfaces. The second, FLUENT (FLUENT, 2006), is based on the finite volume method to solve RANS equations. Volume of Fluid method (VOF) is used for modeling free surface flows. Time integration is achieved by a second order implicit scheme, momentum equations are discretized using MUSCL scheme and HRIC (High Resolution Interface Capturing) scheme is used for convective term of VOF transport equation.

The case study consists of a 10 m deep channel with a 10 m wide chamber at its end. Lip submergence was set to 5 m and its thickness, to 0.5 m. One meter high waves with different periods (5 to 18 seconds) are simulated. Comparisons between FLUINCO and FLUENT results and discussions about the free surface elevation inside the chamber related to its elevation outside the chamber and the flow behavior are presented.

2. NUMERICAL MODELS

2.1. FLUINCO model

2.1.1. Governing equations for fluid flows

Mass conservation for slightly compressible fluids, assuming constant entropy, may be expressed by the following equation:

$$\frac{\partial \rho}{\partial t} + \frac{\partial (\rho v_i)}{\partial x_i} = -\frac{\partial U_i}{\partial x_i} \quad (i=1,2,3), \quad (1)$$

where ρ is the specific mass, c is the sound speed, $U_i = \rho v_i$ and v_i are the fluid velocity components.

Equations expressing both momentum and energy conservation in ALE description complete the governing equations of the fluid flow problem:

$$\frac{\partial (U_i)}{\partial t} + \frac{\partial (f_{ij})}{\partial x_j} + \frac{\partial \rho}{\partial x_i} - \frac{\partial \tau_{ij}}{\partial x_j} - \rho g_i = w_j \frac{\partial (U_i)}{\partial x_j} \quad (i,j=1,2,3), \quad (2)$$

$$\frac{\partial (\rho e)}{\partial t} + \frac{\partial (\rho e v_i)}{\partial x_i} - \frac{\partial}{\partial x_j} \left(k \frac{\partial T}{\partial x_j} \right) = w_j \frac{\partial (\rho e)}{\partial x_j} \quad (i,j=1,2,3), \quad (3)$$

where w_i are the mesh velocity components, T is the temperature, e is the internal specific energy, k is the thermal conductivity and g_i are the gravity acceleration components. $\tau_{ij} = \mu \left(\frac{\partial v_i}{\partial x_j} + \frac{\partial v_j}{\partial x_i} \right) + \lambda \frac{\partial v_k}{\partial x_k} \delta_{ij}$ are the components of the deviatoric tensor, μ and λ are the shear and volumetric viscosity coefficients, respectively, δ_{ij} is the Kronecker delta and $f_{ij} = v_j (\rho v_i) = v_j U_i$. Initial and boundary conditions must be added to Eq. (1), (2) and (3) in order to define the problem uniquely. In incompressible flows, the energy equation, Eq. (3), can be solved independently, after the field of velocities is computed.

2.1.2. Time and space discretizations

The variables U_i are discretized in time domain using a Taylor series expansion. In the first step, corresponding to the time interval $[t^n, t^{n+1/2}]$, U_i are given by the following expression (Teixeira and Awruch, 2001):

$$U_i^{n+1/2} = U_i^n + \frac{\Delta t}{2} \frac{\partial U_i^n}{\partial t} = U_i^n - \frac{\Delta t}{2} \left(\frac{\partial f_{ij}^n}{\partial x_j} - \frac{\partial \tau_{ij}^n}{\partial x_j} + \frac{\partial p^n}{\partial x_i} + \frac{1}{2} \frac{\partial \Delta p}{\partial x_i} - w_j^n \frac{\partial U_i^n}{\partial x_i} \right) (i,j=1,2,3), \quad (4)$$

where $p^{n+1/2} = p^n + 1/2 \Delta p$, with $\Delta p = p^{n+1} - p^n$. Using

$$\tilde{U}_i^{n+1/2} = U_i^n - \frac{\Delta t}{2} \left(\frac{\partial f_{ij}^n}{\partial x_j} - \frac{\partial \tau_{ij}^n}{\partial x_j} + \frac{\partial p^n}{\partial x_i} - w_j^n \frac{\partial U_i^n}{\partial x_i} \right) (i,j=1,2,3). \quad (5)$$

Eq. (4) is given by the following expression:

$$U_i^{n+1/2} = \tilde{U}_i^{n+1/2} - \frac{\Delta t}{4} \frac{\partial \Delta p}{\partial x_i} (i=1,2,3). \quad (6)$$

By discretizing Eq. (1) in time and applying Eq. (6), the result is:

$$\Delta p = \frac{1}{c^2} \Delta p = -\Delta t \frac{\partial U_i^{n+1/2}}{\partial x_i} = -\Delta t \left[\frac{\partial \tilde{U}_i^{n+1/2}}{\partial x_i} - \frac{\Delta t}{4} \frac{\partial}{\partial x_i} \frac{\partial \Delta p}{\partial x_i} \right] (i = 1,2,3). \quad (7)$$

The second step is given by the following expression:

$$U_i^{n+1} = U_i^n + \Delta t \frac{\partial U_i^{n+1/2}}{\partial t} = U_i^n - \Delta t \left(\frac{\partial f_{ij}^{n+1/2}}{\partial x_j} - \frac{\partial \tau_{ij}^{n+1/2}}{\partial x_j} + \frac{\partial p^{n+1/2}}{\partial x_i} - w_j^{n+1/2} \frac{\partial U_i^{n+1/2}}{\partial x_i} \right) (i,j=1,2,3). \quad (8)$$

After space discretization, the flow is analysed by the following algorithm: (a) determine $\tilde{U}_i^{n+1/2}$ with Eq. (5); (b) determine Δp with Eq. (7) and calculate $p^{n+1} = p^n + \Delta p$; (c) determine $U_i^{n+1/2}$ with Eq. (6); and (d) determine U_i^{n+1} with Eq. (8).

The classical Galerkin weighted residual method is applied to the space discretization. In the variables at $t+\Delta t/2$ instant, a constant shape function \mathbf{P}_E is used, and in the variables at t and $t+\Delta t$, a linear shape function \mathbf{N} is employed. By applying this procedure to Eq. (5), (7), (6) and (8), the following expressions in the matrix form are obtained (Teixeira and Awruch, 2001):

$$\Omega_E^{n+1/2} \tilde{\mathbf{U}}_i^{n+1/2} = \mathbf{C} \bar{\mathbf{U}}_i^n - \frac{\Delta t}{2} \left[\mathbf{L}_j (\bar{\mathbf{f}}_{ij}^n - \bar{\boldsymbol{\tau}}_{ij}^n) + \mathbf{L}_i \bar{\mathbf{p}}^n - \mathbf{T} \bar{\mathbf{U}}_i^n - \Omega_E^{n+1/2} \bar{\rho} \bar{\mathbf{g}}_i \right] \quad (9)$$

$$\left(\tilde{\mathbf{M}} + \frac{\Delta t^2}{4} \mathbf{H} \right) \Delta \bar{\mathbf{p}} = \Delta t \left(\mathbf{L}_i^T \tilde{\mathbf{U}}_i^{n+1/2} + \mathbf{f}_a \right) \quad (10)$$

$$\bar{\mathbf{U}}_i^{n+1/2} = \tilde{\mathbf{U}}_i^{n+1/2} - \frac{\Delta t}{4 \Omega_E} \mathbf{L}_i \Delta \bar{\mathbf{p}} \quad (11)$$

$$\mathbf{M}^{n+1} \bar{\mathbf{U}}_i^{n+1} = \mathbf{M}^n \bar{\mathbf{U}}_i^n + \Delta t \left[\mathbf{L}_j^T (\bar{\mathbf{f}}_{ij}^{n+1/2} - \bar{\mathbf{w}}_j^{n+1/2} \bar{\mathbf{U}}_i^{n+1/2}) - \mathbf{Q}_j \bar{\boldsymbol{\tau}}_{ij}^n + \mathbf{Q}_i (\bar{\mathbf{p}}^n + \Delta \bar{\mathbf{p}}/2) + \mathbf{S}_{bi} - \mathbf{C}^T \bar{\mathbf{g}}_i \right] \quad (12)$$

where variables with upper bars at n and $n+1$ instants indicate nodal values, while those at $n+1/2$ instant represent constant values in the element. The matrices and vectors from Eq. (9) to (12) are volume and surface integrals that were obtained by applying the classical Galerkin method. They are expressed by (Teixeira and Awruch, 2001):

$$\begin{aligned} \Omega_E^{n+1/2} &= \int_{\Omega^{n+1/2}} \mathbf{P}_E^T \mathbf{P}_E \, d\Omega & \mathbf{C} &= \int_{\Omega^n} \mathbf{P}_E^T \mathbf{N} \, d\Omega & \mathbf{L}_i &= \int_{\Omega^n} \mathbf{P}_E^T \frac{\partial \mathbf{N}}{\partial x_i} \, d\Omega \\ \mathbf{T} &= \int_{\Omega^n} \mathbf{P}_E^T \mathbf{N} \bar{\mathbf{w}}_i^n \frac{\partial \mathbf{N}}{\partial x_i} \, d\Omega & \tilde{\mathbf{M}} &= \int_{\Omega^{n+1/2}} \mathbf{N}^T \left(\frac{1}{c^2} \right) \mathbf{N} \, d\Omega & \mathbf{H} &= \int_{\Omega^{n+1/2}} \frac{\partial \mathbf{N}^T}{\partial x_i} \frac{\partial \mathbf{N}}{\partial x_i} \, d\Omega \end{aligned} \quad (13)$$

$$\mathbf{f}_a - \int_{\Gamma^{n+1/2}} \mathbf{N}^T \mathbf{P}_E \mathbf{n}_i \tilde{\mathbf{U}}_i^{n+1/2} d\Gamma \quad \mathbf{M}^n = \int_{\Omega^n} \mathbf{N}^T \mathbf{N} d\Omega \quad \mathbf{Q}_i = \int_{\Omega^n} \frac{\partial \mathbf{N}^T}{\partial x_i} \mathbf{N} d\Omega$$

$$\mathbf{S}_{bi} = - \int_{\Gamma^{n+1/2}} \mathbf{N}^T \mathbf{P}_E \mathbf{n}_j d\Gamma \left(\bar{\mathbf{f}}_{ij}^{n+1/2} - \bar{\mathbf{w}}_j^{n+1/2} \bar{\mathbf{U}}_i^{n+1/2} \right)$$

Equation (10) is solved using the conjugated gradient method with diagonal pre-conditioning (Argyris et al., 1985). In Eq. (12), the consistent mass matrix is substituted by the lumped mass matrix, and then this equation is solved iteratively.

2.1.3. Kinematic free surface boundary condition (KFSBC)

The free surface is the interface between two fluids, water and air, where atmospheric pressure is considered constant (generally the reference value is null). In this interface, the KFSBC is imposed. By using the ALE formulation, it is expressed as (Ramaswamy and Kawahara, 1987):

$$\frac{\partial \eta}{\partial t} + \left({}^{(s)}v_i - {}^{(s)}w_i \right) \frac{\partial \eta}{\partial x_i} = 0 \quad (i=1,2,3), \quad (14)$$

where η is the free surface elevation, ${}^{(s)}v_i$ and ${}^{(s)}w_i$ are the fluid and mesh velocity components in the free surface, respectively. The eulerian formulation is used in the x and y directions (horizontal plane) while the ALE formulation is employed in the z or vertical direction.

The time discretization of KFSBC is carried out in the same way as the one for the momentum equations as presented before. After applying expansion in Taylor series, the expressions for η at $n+1/2$ (first step) and $n+1$ (second step) instants are obtained:

$$\eta^{n+1/2} = \eta^n + \frac{\Delta t}{2} \left({}^{(s)}v_3 - {}^{(s)}v_1 \frac{\partial \eta}{\partial x_1} - {}^{(s)}v_2 \frac{\partial \eta}{\partial x_2} \right)^n \quad (15)$$

$$\eta^{n+1} = \eta^n + \Delta t \left({}^{(s)}v_3 - {}^{(s)}v_1 \frac{\partial \eta}{\partial x_1} - {}^{(s)}v_2 \frac{\partial \eta}{\partial x_2} \right)^{n+1/2}$$

The triangular elements coincide with the face of the tetrahedral elements on the free surface. By adopting a linear triangular element and applying the Galerkin method to Eq. (15), these equations can be written as:

$$\int_{A^{n+1/2}} \mathbf{N}_s^T \mathbf{N}_s dA \bar{\eta}^{n+1/2} = \int_{A^n} \mathbf{N}_s^T \mathbf{N}_s dA \bar{\eta}^n + \frac{\Delta t}{2} \left(\int_{A^n} \mathbf{N}_s^T \mathbf{N}_s dA \bar{v}_3^n - \int_{A^n} \mathbf{N}_s^T \mathbf{N}_s dA \left({}^{(s)}\bar{v}_i \frac{\partial \eta}{\partial x_i} \right)^n \right) \quad (16)$$

$$\int_{A^{n+1}} \mathbf{N}_s^T \mathbf{N}_s dA \bar{\eta}^{n+1} = \int_{A^n} \mathbf{N}_s^T \mathbf{N}_s dA \bar{\eta}^n + \Delta t \left(\int_{A^{n+1/2}} \mathbf{N}_s^T \mathbf{N}_s dA \bar{v}_3^{n+1/2} - \int_{A^{n+1/2}} \mathbf{N}_s^T \mathbf{N}_s dA \left({}^{(s)}\bar{v}_i \frac{\partial \eta}{\partial x_i} \right)^{n+1/2} \right)$$

where $i=1,2$; A is the triangular element area, \mathbf{N}_s is the linear shape function, $\bar{\eta}^n$, $\bar{\eta}^{n+1/2}$ and $\bar{\eta}^{n+1}$ are nodal values of elevations at t , $t + \Delta t/2$ and $t + \Delta t$ instants, respectively. Equations (16) are solved in an iterative form in the same way as in the momentum equations.

2.1.4. Mesh movement

The mesh velocity vertical component w_3 is computed to diminish element distortions, keeping prescribed velocities on moving (free surface) and stationary (bottom) boundary surfaces. The mesh movement algorithm adopted in this paper uses a smoothing procedure for the velocities based on these boundary surfaces. The updating of the mesh velocity at point i of the finite element domain is based on the mesh velocity of the points j that belong to the boundary surfaces, and is expressed in the following way (Teixeira and Awruch, 2005):

$$w_3^i = \frac{\sum_{j=1}^{ns} a_{ij} w_3^j}{\sum_{j=1}^{ns} a_{ij}} \quad (17)$$

where ns is the total number of points belonging to the boundary surfaces and a_{ij} are the influence coefficients between the point i inside the domain and the point j on the boundary surface given by the following expression:

$$a_{ij} = \frac{1}{d_{ij}^4} \quad (18)$$

with d_{ij} being the distance between points i and j . In other words, a_{ij} represents the weight that every point j on the boundary surface has on the value of the mesh velocity at points i inside the domain. When d_{ij} is low, a_{ij} has a high value, favouring the influence of points i , located closer to the boundary surface containing point j .

2.2 FLUENT model

The FLUENT-ANSYS program (FLUENT, 2006), version 6.3.26, is based on the finite volume method to solve RANS equations. Unknowns, such as velocity and pressure, are located at the center of the control volumes. The Volume of Fluid method (VOF), based on a capturing technique of free surface, is used for modeling the free surface flow (Hirt and Nichols, 1981). In these simulations, VOF equation is treated implicitly. This method identifies the free surface position through a scalar indicator, named volume fraction, which is equal to 0 for air and 1 for water. The free surface position is defined by value 0.5. Time integration is achieved by a second order implicit scheme. Pressure-velocity coupling is achieved using the SIMPLEC algorithm where under-relaxation factors are all equal to 1, except those related with the turbulence model (these are equal to 0.8). Momentum equations are discretized by using MUSCL scheme (third order scheme). Diffusion term is discretized by a central differencing scheme. Convective term of VOF equation is discretized using the HRIC (High Resolution Interface Capturing) scheme, specially developed for capturing interface. Pressure is calculated by using PRESTO! (PREssure STaggering Option) scheme. Turbulence model K- ϵ is adopted and the convective terms of turbulence equations are discretized by an upwind second order scheme.

3. THE NUMERICAL SIMULATION

3.1 Case study description

The case study consists of a 10 m deep channel with a 10 m wide chamber at its end. The lip submergence was set to 5 m and its thickness, to 0.5 m. The length of the channel is fivefold the wavelength (L). The chamber is open to the atmosphere. Figure 1 shows a sketch of the channel and chamber in the domain as well as the gauge positions. One meter high waves with different periods ($T = 5$ s to 18 s) were simulated. The relation between the depth (h) and the wavelength (L) varies from 1/18 to 1/4, characterizing intermediate waters. The relation between the wavelength (L) and the chamber length (D) ranges from 3.7 to 17.5.

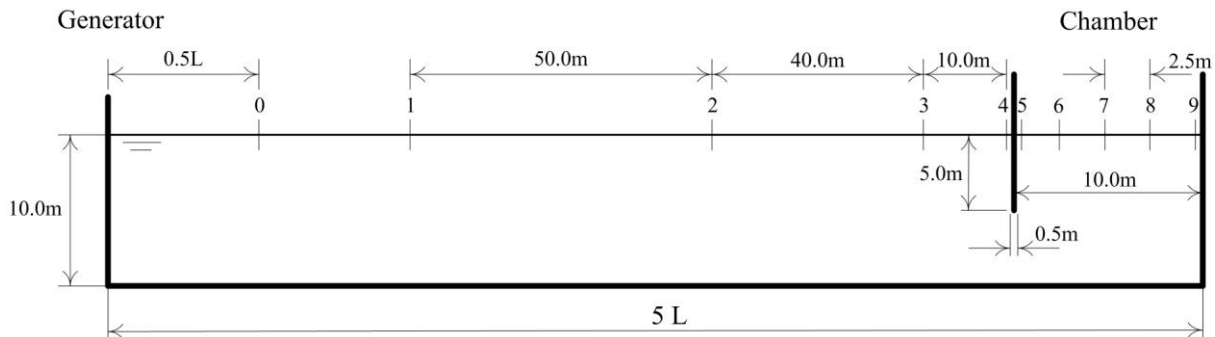


Figure 1. Sketch of the domain and gauge positions

3.2 Simulation conditions

Concerning spatial discretization, forty-four layers in the vertical direction are used for FLUINCO model, being higher on the free surface, bottom and half the depth, where flow disturbance is expected to happen due to the presence

of the lip edge. In the horizontal direction, the size of elements respects the maximum value of $L/50$, where L is the wavelength; near the lip edge, the element sizes are lower. A time step equal to 0.0015 s, which satisfies the Courant limit condition, is used. Waves are generated by imposing the elevation and the velocity components of a linear wave at each instant to the boundary. The non-slip condition is imposed on the bottom and on the walls. CPU time on Intel QuadCore i7 2.80GHz, 8GB memory, 64 bits operational system, is around 2 hours per wave period.

Previous studies have shown that wave propagation in FLUENT is well simulated using 60 elements per wave length and 20 elements in the region of free surface (Barreiro et al, 2009) (Paixão Conde et al., 2009). Consequently, the mesh is constructed using 60 elements per wave length in horizontal direction stretched near the lip edge. There are also 20 elements in vertical direction in the free surface capture zone stretched from this zone to top and bottom, totalizing 41187 quadrilateral elements. Wave generation is simulated by imposing the velocity components and volume fraction (according to the free surface elevation along the time) on the boundary, both defined by the linear wave theory in intermediate water. A non-slip condition is imposed on the bottom, the lip edge and the OWC walls. Finally, atmospheric pressure is imposed on the OWC chamber and the tank top. Time step is equal to $T/600$ and six non-linear iterations per time step enable to reduce the residue by at least two orders of magnitude. CPU time on Intel Core2 Duo 8500 3.16GHz PC (using one core) is around 5 hours per wave period.

3.3 Results and discussion

Comparisons among FLUINCO and FLUENT results are presented in this section. Figures 2 and 3 show the free surface elevation at the center of the chamber for an 8 s and a 10 s wave period, respectively. Results of both models are very close although some small differences in wave amplitude can be observed.

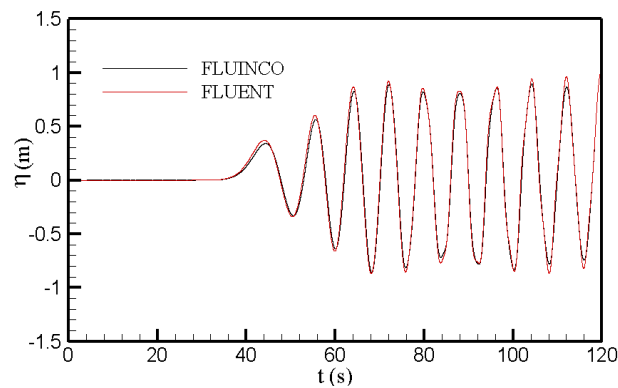


Figure 2. Free surface elevations inside the chamber for $T = 8$ s

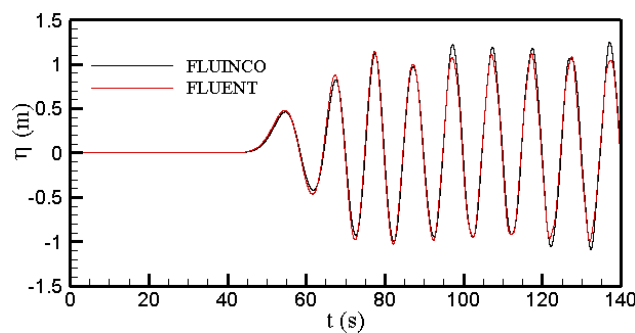


Figure 3. Free surface elevations inside the chamber for $T = 10$ s

Figure 4 shows the velocity vectors and the distribution of the velocity modulus near the lip at a given time and a quarter of a period later for a 7 s period wave. Disturbance of the flow following free surface movement near the tip of the chamber skirt is observed. Again, very similar behavior of the flow is displayed by both models.

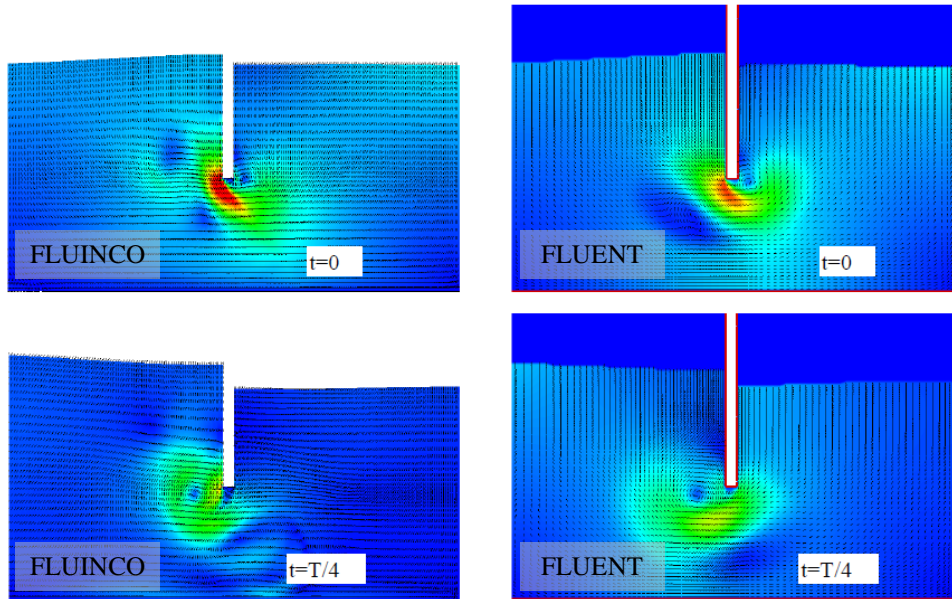


Figure 4. Velocity vectors and distribution of the velocity modulus for 7 s wave period at two instants obtained by FLUINCO and FLUENT

Figures 5 and 6 show streamlines and distribution of the velocity modulus for waves of 7 and 12 s, respectively. Disturbances of the flow near the lip are found to be higher for the 7 s wave, probably due to the fact that free surface elevations inside and outside the chamber are out of phase, as can be seen by the streamlines direction and the graph of the phase angles shown in Fig. 7. In both cases, some vortices, without the presence of turbulence, are observed. The influence of the lip shape in the flow was studied by Horko (2007) in details.

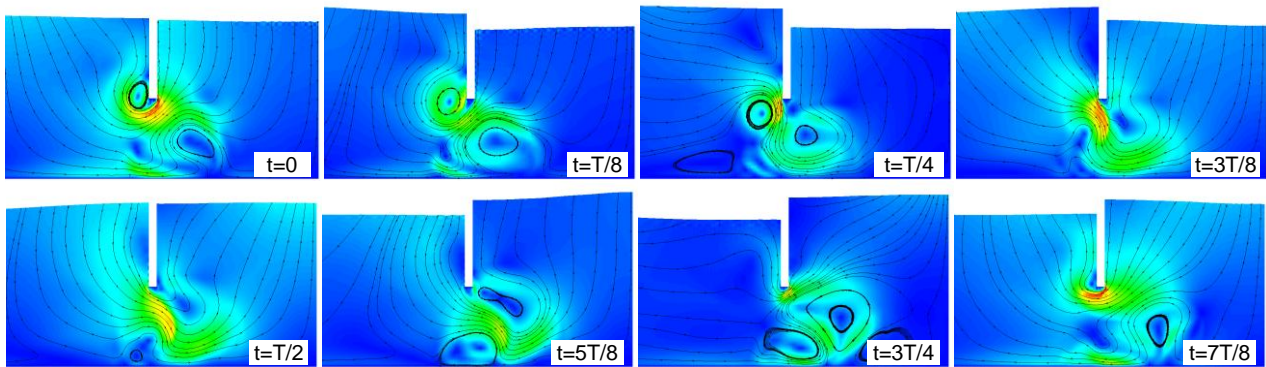


Figure 5. Streamlines and distribution of the velocity modulus for 7 s wave

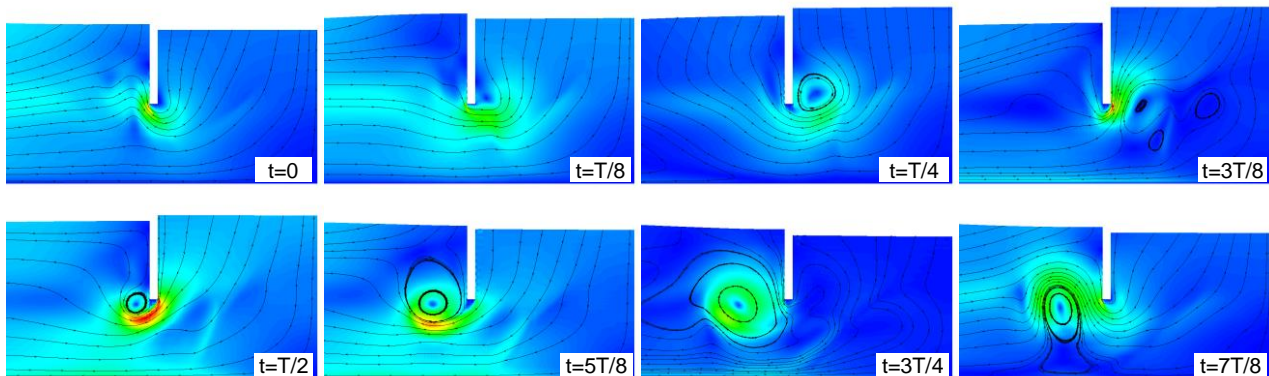


Figure 6. Streamlines and distribution of the velocity modulus for 12 s wave

Figure 7 shows the amplification factor, defined as the ratio between the wave height inside the chamber and the incident wave height. Due to sloshing inside the chamber, a mean water elevation taken among the inner gauges was used for the computation. Below the 7 s wave period, the amplification factor is lower than 1.0; above this value, the amplification rises up to about 15 s and then seems to stabilize. Good agreement between models can be seen, with minor differences around the 10 s and 15 s wave periods.

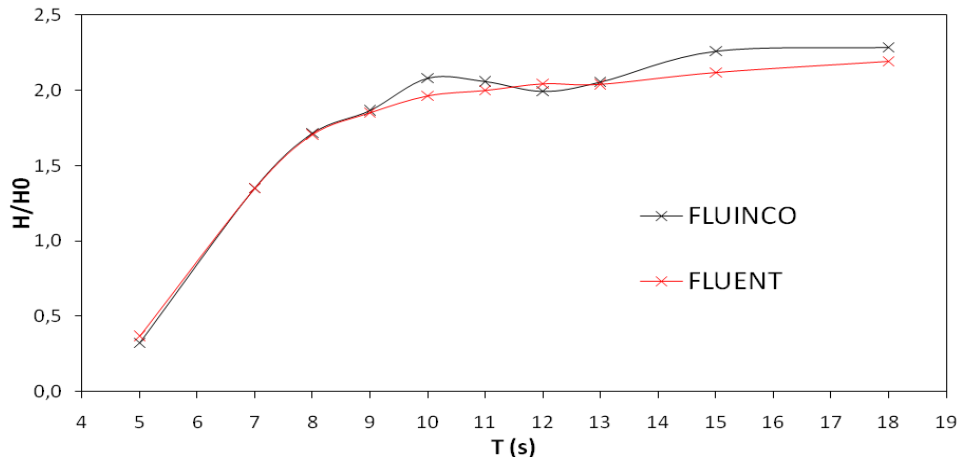


Figure 7. Amplification factor

Figure 8 shows the phase angle (θ), which is the angular difference between the wave inside and outside the chamber, obtained by FLUINCO and FLUENT. Both curves show the same general characteristics. We can observe that the phase angles are smaller (below 30 degrees for FLUINCO and 45 degrees for FLUENT) for higher periods (above 10 s). In this range, amplification factors are higher, between 2 and 2.3. While, for periods below 10 s, angle phases increases, reaching 190 degrees for $T = 5$ s, and amplification factors decrease up to 0.3 for $T = 5$ s.

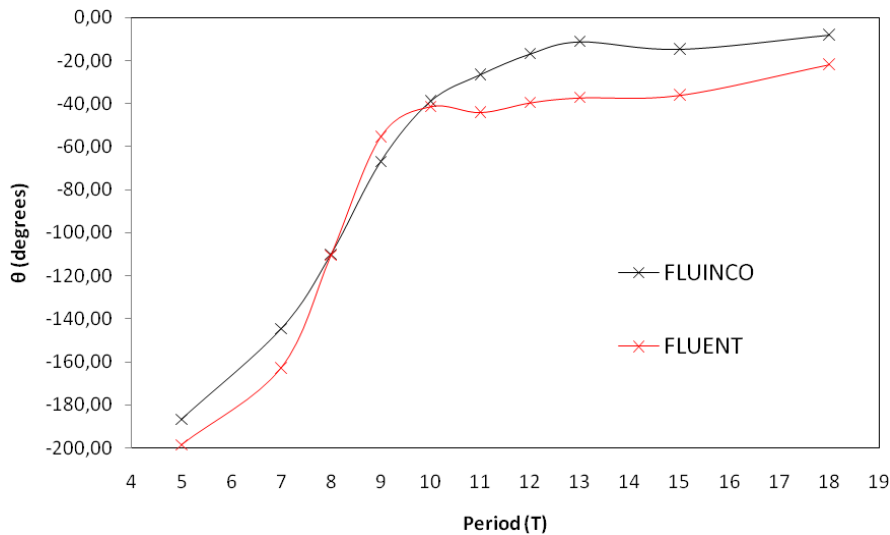


Figure 8. Phase angle (θ)

Figure 9 shows the sloshing parameter (s), defined in this paper as the average of the maximum difference between the free surface elevation inside the chamber at the lip minus the free surface elevation inside the chamber on the right wall. A sloshing peak is found at 7 s, although FLUENT model shows a higher sloshing magnitude than FLUINCO ($s=0.65$ m and 0.5m, respectively). Minor values are found for periods above 11 s (around 0.1m). Nevertheless, the sloshing presents the same behavior for the two codes.

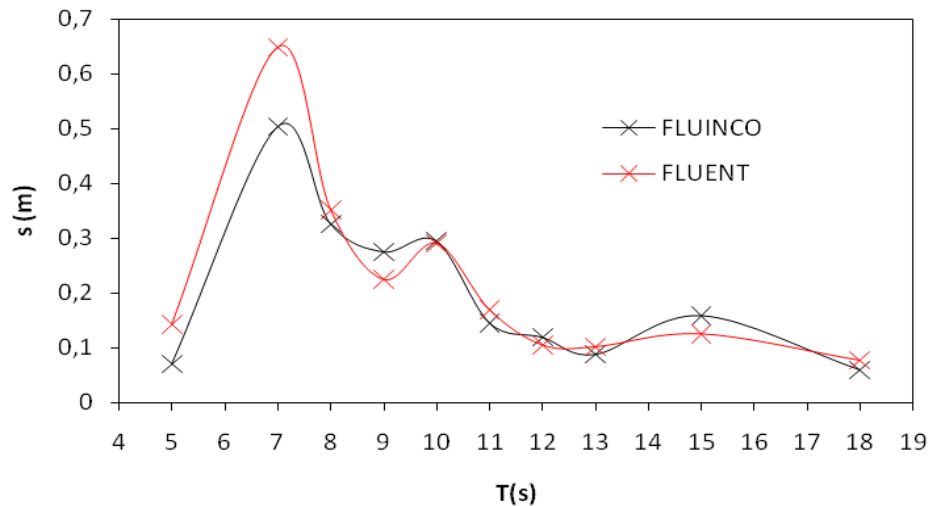


Figure 9. Sloshing parameter

Sloshing phenomena can also be observed by studying the frequency spectrum of the elevations inside the chamber. Figure 10 shows the frequency spectrum of three gauges inside the chamber (front wall, middle, rear wall) for the 7 s and 12 s period waves. On the middle gauge in the 7 s wave, energy is concentrated in the fundamental frequency, the heave frequency, while on the gauges at the extremes of the chamber, a second component can be seen, indicating sloshing. In the 12 s wave, all gauges have almost the same spectrum, energy being concentrated almost solely in the fundamental frequency, which indicates the absence of sloshing.

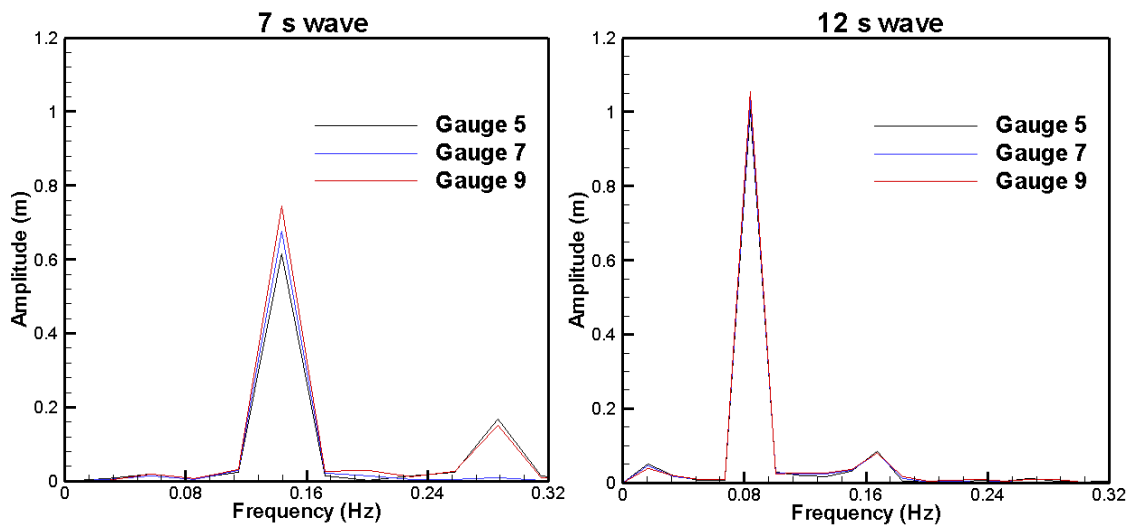


Figure 10. Frequency spectrum for gauges inside chamber for 7 and 12 s period waves

4. CONCLUSIONS

The flow behavior around an onshore OWC energy extraction device was analysed using two numerical models, FLUINCO and FLUENT, based on RANS equations, was presented in this paper. FLUINCO is a code based on semi-implicit two-step Taylor-Galerkin method (Teixeira, 2001). An ALE formulation is used to enable the solution of problems involving movements of free surface. FLUENT (FLUENT, 2006) is based on the finite volume method to solve RANS equations. VOF is used for modeling free surface flows.

Effects of 1 m high waves and different periods from 5 to 18 seconds were simulated. The OWC is placed at the end of a 10 m deep channel that is fivefold longer than the wavelength. The chamber length was set to 10 m and the front lip submergence to 5 m.

Both models have shown similar results in terms of the free surface elevation, the amplification, the sloshing and the flow behavior. Below the 7 s wave period, the amplification factor is lower than 1.0; above this value, the amplification rises up to about 15 s when it stabilizes. Phase angles are smaller (below 30 degrees) for higher periods (above 10 s) whereas, for periods below 10 s, angle phases increase, reaching 190 degrees for $T = 5$ s, and amplification factors

decrease up to 0.3 for $T = 5$ s. The sloshing inside the chamber is higher in the 7 s wave while minor effect is observed for periods above 11 s.

Analyses in this study have shown the phenomena that occur in interactions among an onshore OWC and waves, considering the full Navier-Stokes equations, in which the effects of viscosity are included. OWC geometry and dimensions were established, but future studies are going to include variations of the device dimensions. Simulations were made for cases in which the free surface is subjected to the atmospheric pressure. A future real simulation should consider the influence of a turbine in the air inside the chamber.

5. ACKNOWLEDGEMENTS

The first author wishes to thank CAPES for the post-graduation scholarship.

6. REFERENCES

- Argyris, J., St. Doltsinis, J., Wuestenberg, H., Pimenta, P. M., 1985, Finite element solution of viscous flow problems, Finite Elements in Fluids, Wiley, New York, Vol.6, pp. 89-114.
- Barreiro, T., Didier, E., Gil, L., Alves, M., 2009, "Simulação numérica não linear do escoamento gerado pela interação entre a agitação marítima e conversores pontuais de energia das ondas", Proceedings of the III Conferência Nacional em Mecânica de Fluidos, Termodinâmica e Energia, pp. 157 (10p. CDRom), 17 e 18 de Setembro de 2009, Bragança, Portugal.
- Brito-Melo, A., 2000, Modelação e pré-dimensionamento de centrais de coluna de água oscilante: aplicação à central de energia das ondas do Pico, Açores, PhD Thesis, Instituto Superior Técnico, École Centrale de Nantes.
- Delauré, Y.M.C. and Lewis, A., 2003, "3D Hydrodynamic modeling of fixed oscillating water column wave power plant by a boundary element methods", Ocean Engineering, Vol.30, pp. 309-330.
- Evans, D.V., 1982, "Wave-Power Absorption by Systems of Oscillating Surface Pressure Distributions," J Fluid Mech, Vol.114, pp. 481-499.
- Falcão, A.F. de O., 2009, "Wave energy utilization: A review of the Technologies", Renewable and Sustainable Energy Reviews 14 (2010), pp. 899-918.
- FLUENT-ANSYS, 2006, Fluent 6.3.26 User's Guide.
- Hirt, C.W. and Nichols, B.D., 1981, "Volume of Fluid (VoF) Method for the Dynamics of Free Boundaries", J. Comp. Phys., Vol.39, pp. 201-225.
- Horko, M., 2007, "CFD Optimisation of an Oscillating Water Column Energy converter", Master of Engineering Science Thesis, School of Mechanical Engineering, The University of Western Australia, Australia, 145 p.
- Josset, C. and Clement, A.H., 2006, "A time-domain numerical simulator for oscillating water column wave power plants", Renewable Energy 32 (2007), pp. 1379-1402.
- Paixão Conde, J.M., Didier, E., Teixeira, P.R.F., 2009, "Simulação numérica da interação de uma onda regular com um cilindro submerso: Comparação de três códigos numéricos", Proceedings of the III Conferência Nacional em Mecânica de Fluidos, Termodinâmica e Energia, pp. 172 (9p. CDRom), 17 e 18 de Setembro de 2009, Bragança, Portugal.
- Ramaswamy, R. and Kawahara, M., 1987, "Arbitrary lagrangian-eulerian finite element method for unsteady, convective, incompressible viscous free surface fluid flow", International Journal for Numerical Methods in Fluids, Vol.7, pp. 1053-1075.
- Sarmiento, A.J.N.A. and Falcão, A.F. de O., 1985, "Wave Generation by an Oscillating Surface-Pressure and Its Application in Wave-Energy Extraction," J. Fluid Mech., Vol.150, pp. 467-485.
- Teixeira, P.R.F., 2001, Simulação numérica da interação de escoamentos tridimensionais de fluidos compressíveis e incompressíveis e estruturas deformáveis usando o método de elementos finitos, Porto Alegre, Tese de doutorado, PPGEC-UFRGS.
- Teixeira, P.R.F. and Awruch, A. M., 2001, "Three-dimensional simulation of high compressible flows using a multi-time-step integration technique with subcycles", Applied Mathematical Modelling, Vol.25, pp. 613-627.
- Teixeira, P.R.F. and Awruch, A. M., 2005, "Numerical simulation of fluid-structure interaction using the finite element method", Computers & Fluids, Vol.34, pp. 249-273.
- Zhen Liu, Z., Shi, H. and Beom-Soo Hyun, B.S., 2009, "Practical design and investigation of the breakwater OWC facility in China", Proceedings of the 8th European Wave and Tidal Energy Conference, Uppsala, Sweden.

7. RESPONSIBILITY NOTICE

The authors are the only responsible for the printed material included in this paper.